JOURNAL OF ENGINEERING SCIENCES

Volume 10, Issue 1 (2023)

Chalyj V., Moroz S., Tkachuk A., Zablotskyi V., Trokhymchuk I., Stelmakh A. (2023). Formation of bearings parts waviness in centerless mortise grinding on rigid supports. Journal of Engineering Sciences, Vol. 10(1), pp. A15-A21, doi: 10.21272/jes.2023.10(1).a3

Formation of Bearings Parts Waviness in Centerless Mortise Grinding on Rigid Supports

Chalyj V.[1][0000-0002-6592-6715], Moroz S.[2][0000-0003-4677-5170], Tkachuk A.[2*][0000-0001-9085-7777], Zablotskyi V.[2][0000-0002-2921-0031], Trokhymchuk I.[2][0000-0002-0737-6452], Stelmakh O.[3][0000-0002-9132-6334]

[1] PSC "SKF Ukraine", 34, Bozhenka St., 43017 Lutsk, Ukraine;
[2] Lutsk National Technical University, 75, Lvivska St., 43018 Lutsk, Ukraine;
[3] Beijing Institute of Technology, 5, Zhongguancun St., Haidian Qu, China

Article info:
Submitted: January 31, 2023
Received in revised form: May 10, 2023
Accepted for publication: May 22, 2023
Available online: June 1, 2023

***Corresponding email:**
a.tkachuk@lntu.edu.ua

Abstract. The formation of waviness on the working surfaces of bearing parts is associated with fluctuations in the size of the cut layer of metal and changes in the components of the cutting force. Laplace operators were used to model the centerless grinding system based on the construction of the transfer function and the characteristic equation. It was found that the formation of waviness depends on the position of the hodograph of the movement of the vector of the center of the part in the complex plane, which in turn depends on the geometric parameters of the rigid supports of the centerless grinder machine. This makes it possible, based on hodographs and the angular orientation of their asymptotes, to determine the geometric stability of the process depending on the angles of adjustment of the rigid supports of the grinder machine. Two methodological approaches were used to confirm the correctness of the hypotheses. The first one is a multiplication of wave's hodographs. The second one is regeneration displacement and the coincidence of the combined hodograph of regeneration and waviness displacement mechanisms with the hodograph of infinitely rigid machine displacement. The diagrams which allow choosing geometry of adjustment of rigid support that allows to increase or decrease parameters of certain harmonics are developed. The 3D diagram allows setting the local minima, characterized by acceptable geometric adjustment conditions, providing regulated waviness of the working surfaces of bearing parts.

Keywords: process innovation, adjustment, asymptote, harmonic analysis, hodograph, waviness.

1 Introduction

During the manufacture of roller bearings, the quality of treated rolling surfaces is essential [1]. When grinding the functional rolling surfaces of roller bearing rings, it is necessary to ensure rapid removal of allowance and high processing performance, the final macro-and micro geometric accuracy of the treated surface, and compliance with physical and mechanical requirements [2]. The size of the cut layer during grinding is proportional to the normal grinding force [3]. The formation of the waviness of the details is caused by deviations in the size of the cut layer or changes in the grinding force [4]. Surface roughness depends on the material of the part and the grinding wheel, the productivity of the allowance removal, and the relative speed between the part and the grinding wheel. The grinding force is the main variable for the machining process analysis [5].

The scheme of the dynamic model, which was used to predict both static (geometric) and dynamic stability of the process of centerless grinding on rigid supports, is shown in Figure 1. During the centerless grinding process study, the tangential force vectors of supports *A* and *B* were not considered since they have small values and do not significantly affect the modeling. The components of the grinding forces F_n, F_t, taking into account the force F_G arising from the weight of the part and the force F_M from magnetic retention, form the formation of force vectors of the reactions of the supports F_A, F_B, which is necessary to ensure the static balance of the grinding system. As seen in Figure 1, the center of the part is shifted relative to the center of the support by a small amount (ΔX; ΔY). This is done to ensure permanent contact with the supports of the part. One of the main

parameters of the centerless grinding process that can be controlled is the angles of inclination of the supports (φ_1 and φ_2).

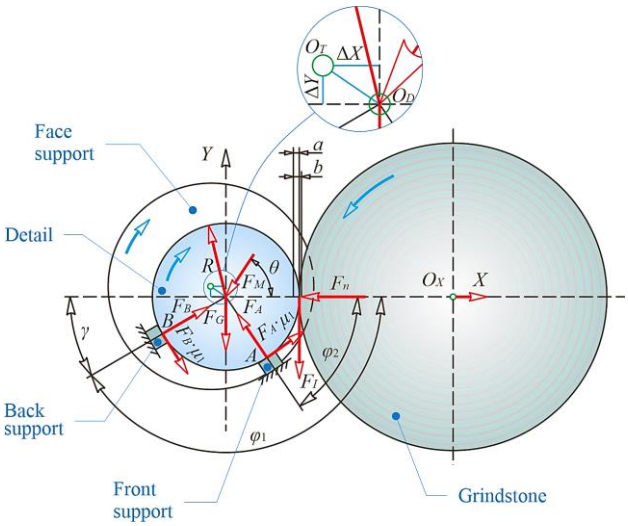

Figure 1 – Scheme of a dynamic model for predicting the stability of the centerless grinding [6]

That is why production requires recommendations for choosing the value of the angles of the supports and obtaining the final regulated harmonics, thanks to this. However, such recommendations require research and scientific justification of their results [6].

2 Literature Review

To research the grinding processes, there are mathematical models used by Laplace operators to analyze the centerless grinding system.

The research of the transfer function and the solution of the characteristic equation is carried out using graph-analytical methods [7]. The formation of waviness depends on the position of the hodograph of the movement of the vector of the center of the detail in the complex plane, which in turn depends on the geometric parameters of the rigid supports of the grinder machine [8, 9]. Adjustment angles φ_1 or φ_2 directly affect the normal component of grinding force, cutting depth, stability in the cutting zone, and, consequently, the harmonics of the newly formed waviness of bearing details [10].

In the Laplace region, multiplication is required to combine the mechanism of waviness and the mechanism of regeneration. For graphical analysis, the mechanism of the combined effect is determined by multiplying the vector by the corresponding value of $s = \sigma + jn$. In this case, the coordinate origin vector for both ripple and regeneration mechanisms is at the same frequency and σ (here, $\sigma = 0$). In vector multiplication, the values of each vector are multiplied, and angles from the positive real axis are added. For example, Figure 2 shows the vector's multiplication at a frequency of $n = 7.5$. The waveform has a magnitude of 2 and an angle of -45°, and the regeneration vector has a magnitude of 3 and an angle of 120°. The combined vector for this condition is shown in Figure 2b, where the value of $n = 7.5$ is the vector 6 (2, 3), and the angle is 75° (120° + (–45°).

The part of the hodograph of the harmonic vector 6 to 8 shows the general picture of the combined hodograph of the vector for different harmonics and conditions set up.

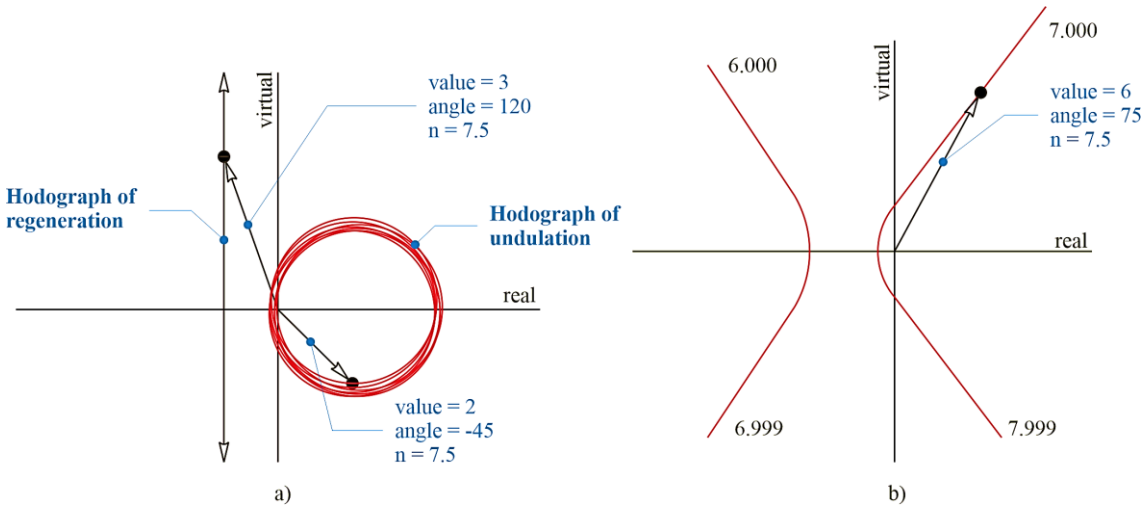

Figure 2 – Vector multiplication scheme (a) and combined hodograph of the vector from 6th to 8th harmonics (b) [6]

Elements of the sample of the combined operation of the hodograph mechanism from the 2nd to the 10th harmonic under a specific debugging condition [11]. These forms of hodograph hyperbola are concentrated around a point (–0.5; 0) in the complex plane and have infinite asymptotes covering the range from 0° to 360° (Figure 3).

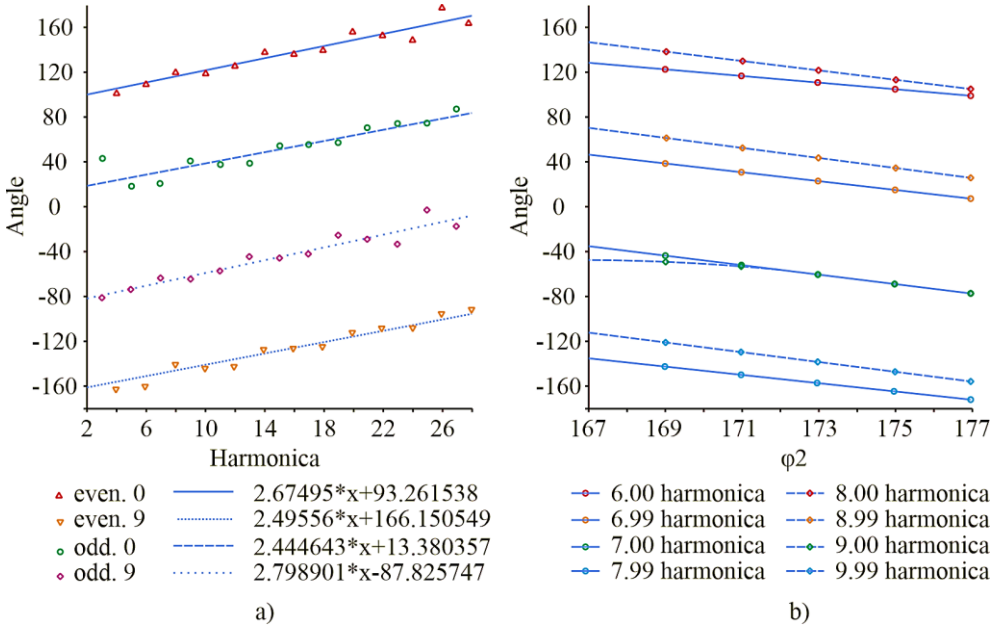

Figure 3 – Vector multiplication scheme (a) and combined hodograph of the vector from 6th to 8th harmonics (b) [11]

Asymptotes have imaginary components, starting with positive infinity for integers numbered harmonics (e.g., 5.000, 6.000) and ending with negative infinity for numbers of smaller integers (e.g., 5.999, 6.999). It is established that the most variable for these hodographs is the angular orientation of the asymptotes. This confirms that the asymptotes around 0° mean the geometric instability of the process [12].

3 Research Methodology

We will analyze the change in waviness harmonics depending on the geometry of the setup of rigid supports (Figure 3a). The asymptotes increase by 2.5° per harmonic with even and odd, grouping at approximately 180° from each other [13, 14].

Figure 3b shows the trends of the asymptotes of the angles with a change in the angle φ_2 for some harmonics if the angle of the front support is constant, $\varphi_1 = 55°$. This graph shows a decrease in the asymptote of the angle if φ_2 is increased. It is also possible to observe even and odd, whole, and next-to-whole asymptotes of angles approximately 180° apart. Since the asymptotes of angles are clear arrays, we need the interpretation of angles to explain the geometry of centerless grinding processes [15, 16].

The study proposes to use two methodologies. The first is the multiplication procedure of hodographs of waviness displacement and regeneration. The second is analyzing the graphic coincidence of the combined hodograph of regeneration and waviness movement mechanisms with the hodograph of infinitely rigid machine movement [17]. The analysis showed that the displacement hodograph has a negative real part, so the mechanism of the waviness effect on the process is unstable [18]. At the same time, the angle of such hodograph movement of the waviness mechanism will acquire a value greater than 90° or less than -90° from the positive real axis. Since the hodograph of the movement of the regeneration mechanism is in a certain area, the angle of the hodograph will be similar at a given frequency. If the waviness and regeneration mechanisms coincide at a certain frequency (geometric angles are compensated), the combined displacement hodograph forms a hyperbola with an asymptote of 0° (-360°). Such a compensation mechanism indicates the geometric instability of the asymptotes for some harmonics [19]. For an infinitely rigid machine, the hodograph of displacement in the complex plane is located at the point at the origin of the coordinates. At the same time, the hodograph of waviness movement and regeneration enters the area around the point (–0.5; 0). The displacement hodographs, which have an asymptote near 0°, usually intersect with the machine displacement hodograph. The fact that the results fall in the system of the process mechanism corresponding to the interaction for this indicated frequency of the ripple allows the growth of this harmonic due to instability in the processing zone [20]. The given interpretation involves an infinitely rigid machine, so the study points to the geometric instability of the waviness frequency, which consists of a vector coincidence in the complex plane. It has been established that the asymptote angles largely depend on the number of harmonics and the geometry of tuning angles, so it allows for predicting which harmonics will be unstable in a given range of tuning angles [21]. Suppose a certain angle of the asymptote of one harmonic is changed and investigated during the full complex of tuning geometry. In that case, it is observed that the theoretical geometric instability of the specified number of harmonics will manifest if the asymptote's

angle is a multiple of the value in radians – 2π. During the research, a contour diagram of the asymptote angle was obtained, and the 14th harmonics were studied within the standard geometry of centerless grinding on rigid supports (Figure 4).

The angular shift from 2π to 0 radians leads to a high density of contours, allowing one to see places where the asymptotes are multiples of 2π easily. This graph shows that the 14th harmonic is theoretically unstable at $\varphi_1 = 52°, 78°$, and $\varphi_2 = 143°, 168°$. Although only one line in each of these regions will be exactly 0°, instability ripples are common for harmonics whose numbers are away from the whole due to a phase shift in the regeneration of waviness regeneration during grinding. Therefore, looking only at the general region, where the whole harmonic is unstable, is best. For example, in Figure 4, an ellipse can be drawn around each area of the concentrated contour lines to represent the main zones where 14th harmonics are theoretically unstable.

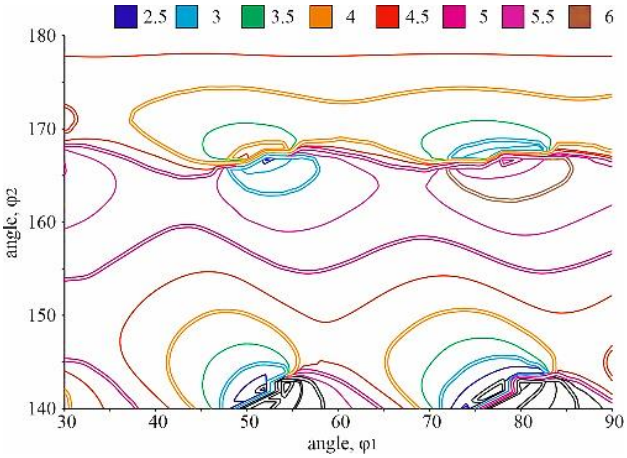

Figure 4 – Contour diagram of asymptote angles in radians for the 14th harmonic within the typical geometry of centerless grinding

During the research, results were obtained that made it possible to construct a diagram of the geometric instability of the waviness for a specific range of harmonics (2–22) for the standard conditions of the geometry of the grinding process adjustment based on the asymptote angles. The diagram confirms that the vast majority of combinations during adjustment of the angles of rigid supports are in the region of geometric instability, and the instability of harmonics corresponds to a particular array of values. For example, consider the 12th harmonic, which is geometrically unstable in the region of $\varphi_1 = 60°$ and $\varphi_2 = 165°$. The 14th harmonic is geometrically unstable in the region above and to the left near the values of $\varphi_1 = 52°$ and $\varphi_2 = 168°$. This diagram allows selecting the geometry of the grinding adjustment on rigid supports, which increases or decreases the parameters of a particular harmonic.

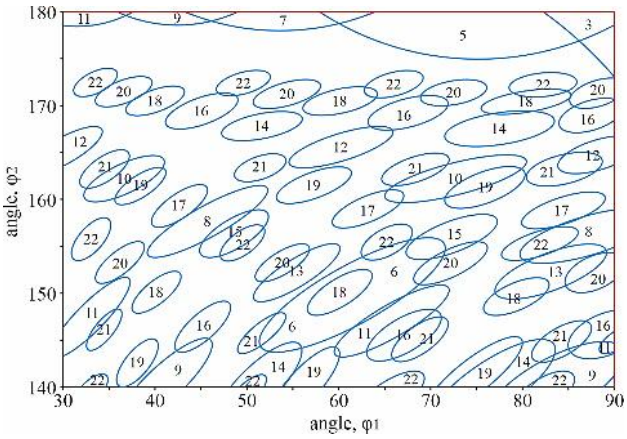

Figure 5 – The geometric instability wave diagram constructed using angular analysis of the combined displacement hodograph at the stability limit within the typical debug geometry

Analysis of Figure 5 makes it possible, with high probability, to predict the geometric instability in the cutting zone during grinding, thereby predicting the growth or reduction of a harmonic ripple.

4 Results

4.1 Impact diagram based on angular analysis of the hodograph

To maintain the stability and relative speed of rotation between the part and the grinding wheel during the machining process, the magnetic force of the end support must be equal to or exceed the tangential grinding force (Figure 1):

$$F_M \geq F_t. \quad (1)$$

The angle of the magnetic force application is equal to

$$\theta \geq arcsin\left(\frac{1}{2 \cdot cos(\gamma)}\right). \quad (2)$$

The geometry of the setup of rigid supports affects the parameters of the waviness of the working surfaces of the roller bearing rings, and different angles of the supports have different effects on the different harmonics of the waviness.

When the combined hodograph of the displacement and regeneration mechanisms for any harmonic had an asymptote at 0°, this harmonic was geometrically unstable. The angles of the asymptotes followed the main trends depending on the machine's adjustment conditions. Given this fact, it is fair to assume that the closer the angle of the asymptote to 0°, the less stable the harmonic becomes. The summary diagram is defined as an indicator of the degree of instability for each debugging condition. When performing this action, there is a need for a parameter that would be proportional to the angle of the asymptote, and angles around 0 or 2π should have a significant effect on it, and angles far from 0 or 2π have little effect. The cosine function satisfies the established requirements. If we take the values of the cosines of the radians shown in Figure 4, the results

diagram suggests a relative level of instability for 14th harmonics under different debugging conditions. In this diagram (Figure 6), contours with levels close to zero (0.1, 0.2) are much more stable than levels around 1.0.

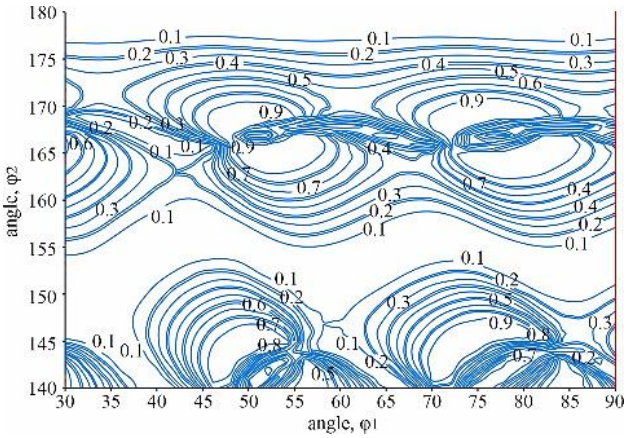

Figure 6 – Contour diagram of cosines of asymptote angles for the 14th harmonic within the typical geometry of centerless grinding

If the performance analysis is similar to Figure 6 for each harmonic from 2 to 30 within the usual geometry of the centerless grinding, we obtain a general diagram of the geometric stability results, shown in Figure 7.

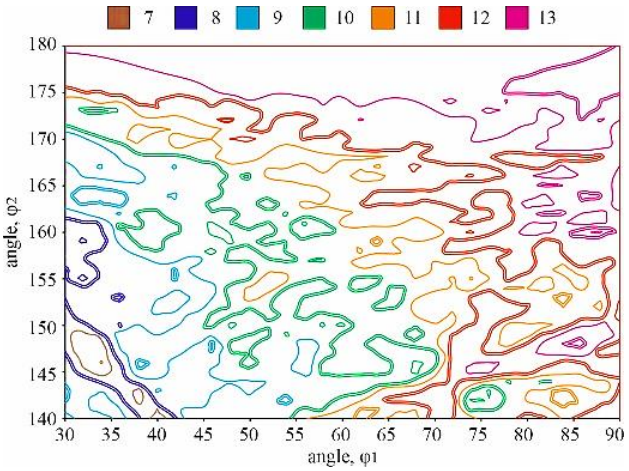

Figure 7 – Contour diagram of all cosines of asymptote angles from 2nd to 30th harmonics within the typical geometry of centerless grinding

4.2 Non-zero sigma, impact diagram based on hodograph diameter analysis

If we analyze the combined hodograph of undulating displacement and regeneration with a non-zero growth rate, σ, its graphical representation changes dramatically. Non-zero σ changes the hodograph of regeneration movement from a straight line to a circle. For a positive σ, the circles are centered closer to the point (–1; 0), while the negative σ forms circles centered around the origin (0; 0).

The size of the hodograph responds faster than the exponential function so that only at the slightest change in the value of σ does it significantly change the appearance of the combined hodograph of waviness displacement and regeneration.

Figure 8 shows a combined hodograph of waviness displacement and regeneration with different positive σ from 6.000 to 7.999 harmonics under a given debugging condition. Thus, the hyperbola rotates around itself, forming cyclic spirals. As the sigma value increases, the size of the spirals decreases. With an absolute increase in the sigma, the size of the spirals decreases.

An infinitely rigid machine in the complex plane is the point at the origin. When the hodograph of the movement of the waviness and regeneration intersects with the hodograph of the movement of this machine, the result is a geometric instability in the grinding zone. If a particular spiral intersects with the hodograph of the machine movement, it should be small enough to be near the origin. Therefore, any value of σ that can make the spiral small enough to intersect with the hodograph of the machine movement will form individual harmonics of unstable level. That is, if one helix is large compared to another at a certain σ, it is clear that a larger helix will need a larger σ to become small enough to intersect with the hodograph of machine movement. On the other hand, the best condition for grinding will result from the debugging condition, the spirals of which form a very small instability (small σ) intersecting with the hodograph of the machine movement. Based on this analysis, the debugging condition with large spirals is less desirable than with smaller spirals at a certain unstable σ.

After using these features, an estimate of the geometric stability of the grinder is obtained based on the size of the combined hodograph of waviness displacement and regeneration at constant, non-zero σ. If we consider in the complex plane of the spiral of all harmonics under all debugging conditions with some non-constant σ, the total size of the spirals will be proportional to the instability under each debugging condition. Figure 9 illustrates the sum of the total size of the spirals from the 2nd to 30th harmonics for each debugging condition within the normal geometry of debugging centerless grinding.

A 3D diagram is shown for the conceptual interpretation of research results.

To analyze the waviness of the raceways of the bearing rings, it is advisable to use the Fourier series, which describes it as a complex periodic function consisting of simple harmonic oscillations with frequencies that are multiples of the fundamental one. The sequence number of a simple harmonic determines the number of irregularities highlighted on the part's surface. In particular, the second term of the Fourier series corresponds to the second harmonic and reflects the ovality of the part's surface, the third term - the third harmonic – reflects the trihedron, and so on.

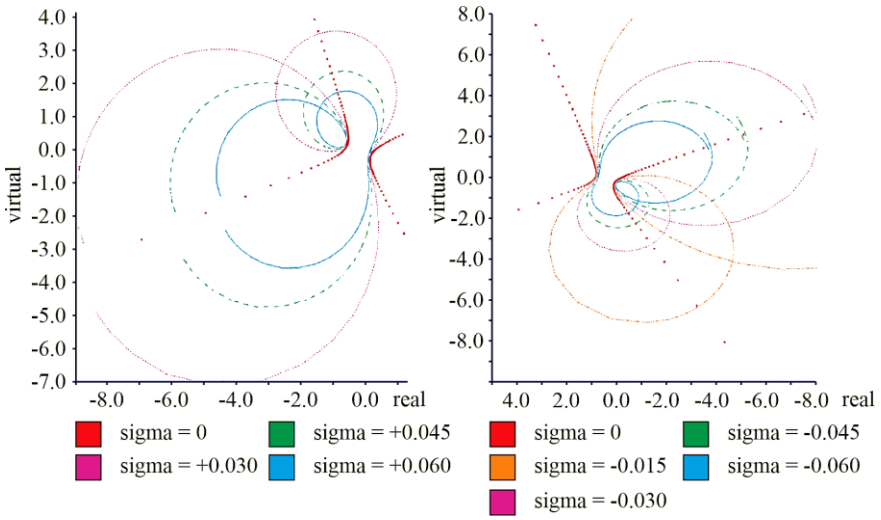

Figure 8 – Scheme of change of the combined hodograph of movement in a spiral at +sigma (a) and at -sigma (b)

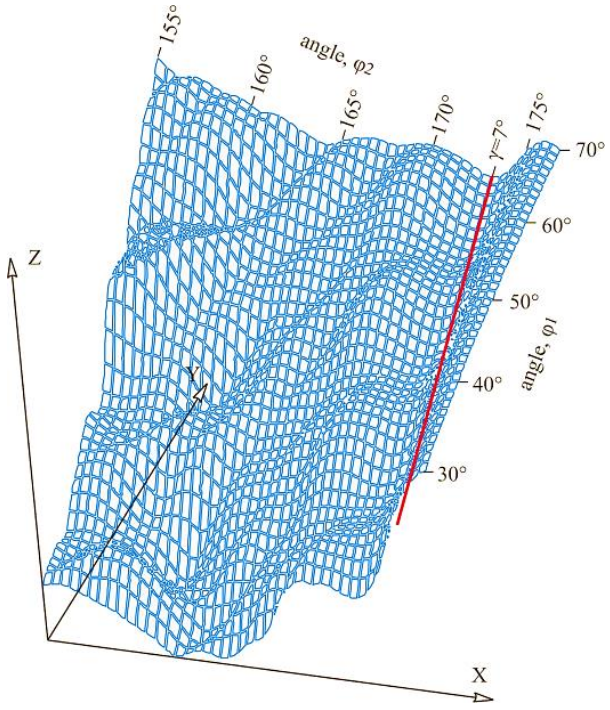

Figure 9 – Scheme of change of the combined hodograph of movement in a spiral at +sigma (a) and at -sigma (b)

5 Conclusions

So, as a result of the conducted research, it was established that the characteristics of the waviness of the working surfaces of the roller bearing rings are influenced by the geometry of the setup of rigid supports during centerless grinding. It is shown that different support angles during processing have different effects on the harmonics of the waviness of the working surfaces of roller bearings.

The mechanism of waviness on the surface of the part in the process of centerless mortise grinding depends on many additional factors (characteristics of the grinding wheel, machine vibration, grinding force, initial and time-varying waviness of the part), which must be considered to ensure stable quality.

The geometry of the rigid supports influences the stability of the centerless grinding process. The corresponding diagrams show this. In particular, on the influence diagram based on the angular analysis of the hodograph, provided that the system finds a stability limit $\sigma = 0$, lower values of the adjustment angles φ_1 and φ_2 lead to greater geometric stability.

In the impact diagram based on the angular analysis of the hodograph, under some level of system instability, it is also observed that smaller adjustment angles φ_1 and φ_2 provide greater geometric stability and should lead to improved surface roughness on a dynamically stable machine. In particular, there is a constant local depression about $\varphi_2 = 173°$ ($\gamma = 7°$), which may be the most optimal condition for centerless grinding. There are several local minima in the diagram, which indicate the presence of several acceptable geometric debugging conditions that provide regulated waviness of the detail.

If the machine is dynamically stable from the point of view of vibration, then according to the general diagram of geometric stability, it is possible to predict trends of final waviness parameters based on the geometry of adjustment of rigid supports at centerless mortise grinding. The results of this study create the preconditions for controlling the parameters of the waviness of bearing detail. It will stabilize bearing parameters such as noise and vibration.

References

1. Yue, Q., Li, L., Zhang, X. (2023). Failure mechanism and bearing capacity analysis of the underpinning structure with relative displacement. *Engineering Failure Analysis*, Vol. 148, 107205, https://doi.org/10.1016/j.engfailanal.2023.107205
2. Gu, Q., Deng, Z., Lv, L., Liu, T., Teng, H., Wang, D., Yuan, J. (2021). Prediction research for surface topography of internal grinding based on mechanism and data model. *International Journal of Advanced Manufacturing Technology*, Vol. 113(3-4), pp. 821-836, https://doi.org/10.1007/s00170-021-06604-7
3. Zhao, B., Wang, X., Ding, W., Wang, Y., Fu, Y., Zhao, Y., Zhu, J. (2023). Grain erosion wear properties and grinding performance of porous aggregated cubic boron nitride abrasive wheels. *Chinese Journal of Aeronautics*, https://doi.org/10.1016/j.cja.2022.08.005
4. Wu, Z., Zhang, L. (2023). Analytical grinding force prediction with random abrasive grains of grinding wheels. *International Journal of Mechanical Sciences*, Vol. 250, 108310, https://doi.org/10.1016/j.ijmecsci.2023.108310
5. Kishore, K., Sinha, M. K., Chauhan, S. R. (2023). A comprehensive investigation of surface morphology during grinding of Inconel 625 using conventional grinding wheels. *Journal of Manufacturing Processes*, Vol. 97, pp. 87-99 https://doi.org/10.1016/j.jmapro.2023.04.053
6. Chalyj, V., Moroz, S., Ptachenchuk, V., Zablotskyj, V., Prystupa, S. (2020). Investigation of waveforms of roller bearing's working surfaces on centerless grinding operations. *In: Ivanov V. et al. (eds) Advances in Design, Simulation and Manufacturing III. DSMIE 2020. Lecture Notes in Mechanical Engineering, Springer, Cham*, Vol. 1, pp. 349-360, https://doi.org/10.1007/978-3-030-50794-7_34
7. Kalchenko, V., Yeroshenko, A., Oyko, S. (2017). Mathematical modeling of abrasive grinding working process. *Naukovyi Visnyk Natsionalnoho Hirnychoho Universytetu*, Vol. 6, pp. 76-82.
8. Zhang, X.-M., Zhang, Q.-J. (2010). Research on the simulation of centerless grinding process. *Proceedings of the 29th Chinese Control Conference*, Vol. 2010, pp. 5310-5313.
9. Chunjian, H., Qiuju, Z., Yubing, X. (2010). Research on the computer simulation technique of cylindrical centerless grinding process. *2010 Second International Workshop on Education Technology and Computer Science*, pp. 431-433, https://doi.org/10.1109/ETCS.2010.551
10. Yang, H., Zhang, L., Li, D., Li, T. (2011). Modeling and analysis of grinding force in surface grinding. *2011 IEEE International Conference on Computer Science and Automation Engineering*, pp. 175-178, https://doi.org/10.1109/CSAE.2011.5952448
11. Zablotskyi, V., Tkachuk, A., Prozorovskyi, S., Tkachuk, V., Waszkowiak, M. (2022). Influence of turning operations on waviness characteristics of working surfaces of rolling bearings. *In: Ivanov, V., Trojanowska, J., Pavlenko, I., Rauch, E., Peraković, D. (eds) Advances in Design, Simulation and Manufacturing V. DSMIE 2022. Lecture Notes in Mechanical Engineering. Springer, Cham*, pp. 345-354, https://doi.org/10.1007/978-3-031-06025-0_34
12. Shah, H., Taha, E. H. (2022). Busemann functions in asymptotically harmonic Finsler manifolds. *Journal of Mathematical Physics, Analysis, Geometry*, Vol. 18(4), pp. 546-561, https://doi.org/10.15407/mag18.04.546
13. Zhuang, J., Cao, Y., Jia, M., Zhao, X., Peng, Q. (2023). Remaining useful life prediction of bearings using multi-source adversarial online regression under online unknown conditions. *Expert Systems with Applications*, Vol. 227, 120276, https://doi.org/10.1016/j.eswa.2023.120276
14. Gabor, M., Zdunek, R., Zimroz, R., Wodecki, J., Wylomanska, A. (2023). Non-negative tensor factorization for vibration-based local damage detection. *Mechanical Systems and Signal Processing*, Vol. 198, https://doi.org/10.1016/j.ymssp.2023.110430
15. Chen, J., Lin, C., Yao, B., Yang, L., Ge, H. (2023). Intelligent fault diagnosis of rolling bearings with low-quality data: A feature significance and diversity learning method. *Reliability Engineering and System Safety*, Vol. 237, https://doi.org/10.1016/j.ress.2023.109343
16. Bai, X., Zeng, S., Ma, Q., Feng, Z., An, Z. (2023). Intelligent fault diagnosis method for rolling bearing using WMNRS and LSSVM. *Measurement Science and Technology*, Vol. 34(7), https://doi.org/10.1088/1361-6501/acc3b9
17. Zhu, D., Yin, B., Teng, C. (2023). An improved spectral amplitude modulation method for rolling element bearing fault diagnosis. *Journal of the Brazilian Society of Mechanical Sciences and Engineering*, Vol. 45(5), https://doi.org/10.1007/s40430-023-04184-z
18. Chen, S., Xie, B., Wang, Y., Wang, K., Zhai, W. (2023). Non-stationary harmonic summation: A novel method for rolling bearing fault diagnosis under variable speed conditions. *Structural Health Monitoring*, Vol. 22(3), pp. 1554-1580, https://doi.org/10.1177/14759217221110278
19. Lin, S., Jiang, S. (2022). Rotordynamics of an improved face-grinding spindle: Rotational stiffness of thrust bearing increases radial stiffness of spindle. *Journal of Manufacturing Science and Engineering, Transactions of the ASME*, Vol. 144(8), https://doi.org/10.1115/1.4053458
20. Zmarzły, P. (2022). Analysis of technological heredity in the production of rolling bearing rings made of AISI 52100 steel based on waviness measurements. *Materials*, Vol. 15(11), https://doi.org/10.3390/ma15113959
21. Brosed, F. J., Zaera, V. A., Padilla, E., Cebrián, F., Aguilar, J. J. (2018). In-process measurement for the process control of the real-time manufacturing of tapered roller bearings. *Materials*, Vol. 11(8), https://doi.org/10.3390/ma11081371